

# High-order Harmonic Generation in a Time-integrated Quantum Transition Picture

Y. J. Chen<sup>1,2</sup>, J. Liu<sup>1,3\*</sup>, and Bambi Hu<sup>2,4</sup>

*1. Institute of Applied Physics and Computational Mathematics, Beijing 100088, China*

*2. Department of Physics, Centre for Nonlinear Studies,*

*and The Beijing-Hong Kong-Singapore Joint Center for Nonlinear and Complex Systems (Hong Kong),  
Hong Kong Baptist University, Kowloon Tong, Hong Kong, China*

*3. Center for Applied Physics and Technology, Peking University, Beijing 100084, China*

*4. Department of Physics, University of Houston, Houston, Texas 77204-5005.*

(Dated: November 2, 2018)

We develop a numerical scheme to investigate the high-order harmonic generation (HHG) in intense laser-matter interactions. Tracing the time evolution of every electronic laser-field-free state, we "observe" the HHG in a time-integrated quantum transition picture. Our full-quantum simulations reveal that continuum electrons with a broad energy distribution contribute equally to one harmonic and the excited state also plays an important role in the molecular HHG. These results imply a laser-intensity-dependent picture of intramolecular interference in the HHG.

PACS numbers: 42.65.Ky, 32.80.Rm

Owing to the important applications in producing burst of high energy photon, high-order harmonic generation (HHG) is a main focus of intense laser-matter physics[1]. In recent years, it is also shown that the HHG can be used to image molecular orbital[2]. The HHG can be well understood by a semiclassical recollision model[3]: (i) ionization of the active electron by tunnelling; (ii) acceleration of the electron in the laser field; (iii) recombination of the electron into the bound state to emit a high energy photon. Another widely used approach to describe the HHG is the strong field approximation (SFA)[4], which can be regarded as the quantum-mechanism version of the semiclassical recollision model.

Numerical investigation on the HHG of  $H_2^+$  demonstrates an interesting phenomenon: a minimum appears in the HHG spectrum that relates to the molecular orientation. Using a point-emitter model, the minimum is identified as arising due to intramolecular two-center interference and the position of the minimum is concluded not to rely on the laser intensity[5]. This minimum has generated great theoretical and experimental interests[6, 7, 8, 9, 10, 11, 12, 13, 14]. Two experimental groups reported the observations of the minima in the HHG spectra of  $CO_2$ [7, 8]. They attributed the minima to two-center interference. However, the positions of the minima are different in their measurements (the 27th vs the 33rd orders). Other than interference, the theoretical calculations proposed that the ground state depletion is also a possible mechanism for the different modulations observed[9]. Zhou et al showed that two-center interference is responsible for the minima in the HHG spectra of  $CO_2$  measured in their experiments[12]. Nevertheless, they found that the interference pattern is subjected to the Coulomb effects. Very recently, the experimental observations of the interference minima in the HHG spectra of  $H_2$  were reported[14]. But the minima are found to be related to the laser intensity. This relation is attributed to the motion of the parent nuclei there. All these strongly call for a revisit of the HHG, especially, a

quantitative description of intramolecular interference in the HHG.

The core of the HHG is the recombination process and the recombination is an intermediate process that can not be observed experimentally. In addition, the semiclassical models that omit the Coulomb effects can not describe the HHG quantitatively. Thus, in this paper, we develop a numerical scheme to investigate the process. We directly solve the Born-Oppenheimer time-dependent Schrödinger equation (TDSE), and we project the wavefunction on the eigen-states of the field-free Hamiltonian and trace its temporal evolution. With the method, we achieve a time-integrated quantum transition picture of the HHG. It gives us direct information about the elaborate role of every electronic state in the HHG and allows us to identify the whole energy transfer among harmonics, the laser field and the electrons in the HHG. Our simulations reveal that the major contributions to one harmonic come from continuum electrons with a broad energy distribution and the first excited state also has a significant contribution to the molecular HHG. As a result, the position of the interference minimum is affected by the laser intensity in the frozen nuclei case.

Below, our discussion is first made for the 1D case, we then validate the main results to the 2D and 3D cases. The Hamiltonian of model molecules  $H_2^+$  or hydrogen-like atoms, all with the ionization potential  $I_p = 1.11$  a.u. studied here, is  $H(t) = \mathbf{p}^2/2 + V(\mathbf{r}) - \mathbf{r} \cdot \mathbf{E}(t)$  (in a.u.  $\hbar = e = m_e = 1$ ). Here,  $V(\mathbf{r})$  is the Coulomb potential. In the 1D and 2D cases, we use the soft-Coulomb potential  $V(x) = \frac{-Z}{\sqrt{1.44+(x+R/2)^2}} + \frac{-Z}{\sqrt{1.44+(x-R/2)^2}}$  and  $V(x, y) = \frac{-Z}{\sqrt{0.5+(x+R/2)^2+y^2}} + \frac{-Z}{\sqrt{0.5+(x-R/2)^2+y^2}}$ , respectively, where  $Z$  is the effective charge,  $R$  is the internuclear separation. For  $H_2^+$ ,  $R = 2$  a.u.  $R = 0$  a.u. corresponds to the hydrogen-like atom. In the case of the 3D atom, it is  $V(\mathbf{r}) = -Z/r$ .  $\mathbf{E}(t) = \vec{\epsilon}\mathcal{E} \sin \omega_0 t$  is the external electric field with the amplitude  $\mathcal{E}$  and the frequency  $\omega_0$ .  $\vec{\epsilon}$  is the unit vector along the laser polarization. We

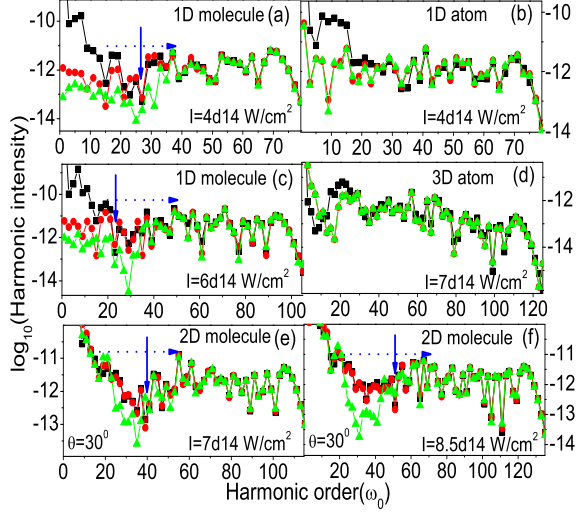


Figure 1: Harmonic spectra of  $\text{H}_2^+$  molecules [(a),(c),(e),(f)] and hydrogen-like atoms [(b),(d)] calculated using different methods. The black curves denote the results obtained using Eq. 1, the red and green curves denote those obtained using Eq. 2 with  $n' = 0, 1$  and  $n' = 0$ , respectively. For the 2D and 3D cases in (d)-(f), also see the context for the details.

use  $\theta$  to denote the angle between the molecular axis and the laser polarization. Our calculation will be performed for 780 nm trapezoidally shaped laser pulses with a total duration of 10 optical cycles and linear ramps of three optical cycles. The details of solving the 1D and 2D TDSE can be found in Ref.[15]. The 3D TDSE is solved following the program described in Ref.[16]. The coherent part of the HHG spectrum is obtained by[5]

$$F(\omega) = \int \langle \psi(t) | \vec{\epsilon} \cdot \nabla V | \psi(t) \rangle e^{i\omega t} dt, \quad (1)$$

where  $|\psi(t)\rangle$  is the time-dependent wavefunction of  $H(t)$ , and  $\omega$  is the emitted proton frequency.

To achieve a full-quantum description of the recombination in the 1D case, we project the wavefunction  $|\psi(t)\rangle$  on the eigen-states of the field-free Hamiltonian  $H_0 = \mathbf{p}^2/2 + V(x)$ , that is  $|\psi(t)\rangle = \sum_n a_n(t) |n\rangle + \int d\mathbf{p} c_{\mathbf{p}}(t) |\mathbf{p}\rangle$ . Here,  $\psi_c(\mathbf{r}, t) = \int d\mathbf{p} c_{\mathbf{p}}(t) |\mathbf{p}\rangle$  represents the continuum electronic wave packet.  $|n\rangle$  is the bound state of  $H_0$  with negative eigen-energy  $E_n$ ;  $|\mathbf{p}\rangle$  represents the continuum state of  $H_0$  that has positive eigen-energy denoted by  $E_{\mathbf{p}}$ . The eigen-states and eigen-values are obtained by numerically diagonalizing the Hamiltonian  $H_0$ .

The recombination in the HHG can be simulated by the evaluation of the dipole movement between the "concerned" bound states and the continuum electronic wave packet  $\psi_c(\mathbf{r}, t)$ , i.e.,  $D(t) = \sum_n a_{n'}^*(t) \langle n' | \nabla V | \psi_c(\mathbf{r}, t) \rangle$ . Here,  $n'$  indicates the concerned bound state that the continuum electrons can transit back to. Because the

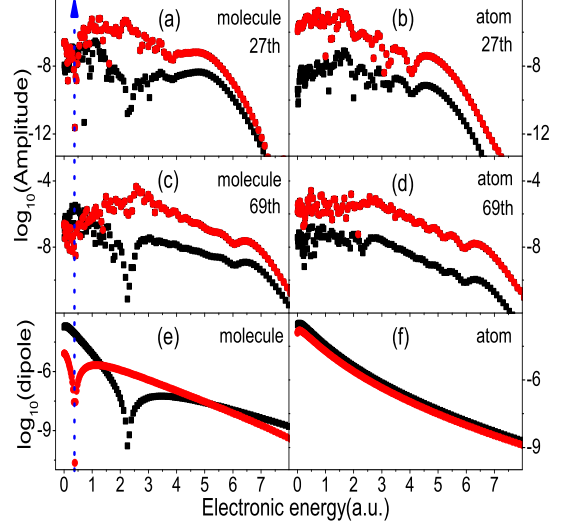


Figure 2: The contribution of  $|G_{n'}(\mathbf{p}, \omega)|^2$  to certain single harmonic orders [(a)-(d)] and the related transition dipoles  $\langle n' | \nabla V | \mathbf{p} \rangle$  [(e)-(f)] for the spectra in Fig. 1(a) and (b). The red curves denote the results obtained with  $n' = 0$ , the black curves denote those obtained with  $n' = 1$ .

population of other higher bound states is found to be negligible in our simulations. In this paper, we focus on the dipole movement in the cases of  $n' = 0$  and  $n' = 0, 1$ , i.e., the dipole movement relating to the transition back to the ground state  $|0\rangle$  and to both the ground state  $|0\rangle$  and the first excited state  $|1\rangle$ . The Coulomb effects, the ground state depletion, and the contribution of higher bound states those are omitted in the SFA, have been accurately incorporated into the expression of  $D(t)$ .

The Fourier transformation of  $D(t)$  gives the complex amplitude describing the HHG at the frequency  $\omega$

$$F(\omega) = \int dt D(t) e^{i\omega t} = \int d\mathbf{p} G(\mathbf{p}, \omega), \quad (2)$$

where  $G(\mathbf{p}, \omega) = \sum_{n'} G_{n'}(\mathbf{p}, \omega)$  and

$$G_{n'}(\mathbf{p}, \omega) = \langle n' | \nabla V | \mathbf{p} \rangle \int dt a_{n'}^*(t) e^{i\omega t} c_{\mathbf{p}}(t). \quad (3)$$

Here,  $\langle n' | \nabla V | \mathbf{p} \rangle$  is the transition dipole matrix element between the continuum  $|\mathbf{p}\rangle$  and the bound state  $|n'\rangle$ .

Eq. 2 shows that the contributions to one harmonic  $\omega$  come from the "returned" continuum electrons with varied energy  $E_{\mathbf{p}}$ , each of which is weighted by the probability amplitude  $G(\mathbf{p}, \omega)$ . The HHG picture revealed here is somewhat different from the semiclassical ones. The electronic momentum in the semiclassical models is the instant momentum that is modulated by the laser field. The momentum in Eq. 2 is the "laser-field-free" momentum. Thus, Eq. 2 implies a "static" quantum

transition picture of the HHG, i.e., the transition of the continuum electron  $|\mathbf{p}\rangle$  with the time-integrated amplitude  $G_{n'}(\mathbf{p}, \omega)$  back to the bound state  $|n'\rangle$ . From the "static" picture, we can read some important messages of the recombination, as shown below.

In Fig. 1(a) and (b), we compare the harmonic spectra of 1D  $\text{H}_2^+$  and its reference atom, calculated using Eq. 1 and Eq. 2, respectively. We expect that the comparison can give an insight into the mechanism of the HHG[15]. First, we see the black curve in Fig. 1(a) for  $\text{H}_2^+$  shows a pronounced suppressed region, i.e., a broad hollow around the 27th order indicated by a dotted arrow. This striking hollow structure is a two-center interference characteristic of the molecular HHG spectrum and will be discussed in detail below. In addition, the red curves in Fig. 1(a) and (b) basically reproduce the behavior of the corresponding black curves in the plateau region. This verifies the applicability of Eq. 2. The difference in the low energy region is due to the omission in Eq. 2, the bound-bound transitions. Especially, in Fig. 1(a), the green curve obtained with  $n' = 0$  (i.e., ignore the first excited state) shows a deeper hollow than the red one that includes the first excited state. In Fig. 1(b) of the atomic case, the two curves are also analogous. Thus, Fig. 1(a) and (b) reveal a main result of this present paper that the first excited state, which is usually omitted in the HHG, could play an important role in the molecular HHG in the hollow regime.

Next, we explore the quantum mechanism behind these phenomena. Fig. 2 plots the contribution of  $|G_{n'}(\mathbf{p}, \omega)|^2$  to certain single harmonics and the corresponding transition dipoles  $\langle n'|\nabla V|\mathbf{p}\rangle$  for the spectra in Fig. 1(a) and (b). We choose two typical harmonic orders, the 27th and 69th, that locate at the interference regime and plateau regime of the HHG spectrum in Fig. 1(a), respectively. Fig. 2(a)-(d) obviously show that for the atomic cases, the amplitude is mainly contributed from the electrons that return to the ground state. For the molecular cases, electrons that transit back to either the ground state or the first excited state could contribute the amplitude significantly, especially in the low energy regime.

The red curves of  $|G_0(\mathbf{p}, \omega)|^2$  in Fig. 2(a) and (c) of the molecular cases show a dip structure around energy  $E(\mathbf{p}) = 0.35$  a.u., indicated by a blue arrow. The black curves of  $|G_1(\mathbf{p}, \omega)|^2$  show similar structures except that the position of the dip structure shifts to a higher electronic energy of 2.25 a.u.. Because its amplitude is small, we can safely ignore its contribution in the following discussion. The first dip that locates at  $E(\mathbf{p}) = 0.35$  a.u. is important and corresponds to the pole of the molecular transition dipole in Fig. 2(e). The latter is believed to be relevant to two-center interference of the diatomic molecules[15, 17]. As we integrate the amplitude over electron energy, this "two-center interference effect" remains visible for the case of the 27th, whereas it vanishes for the case of the 69th, as presented in Fig. 3(a)-(d).

In the left panels of Fig. 3, we plot the integrated contribution of  $|\sum_{n'} \int_0^{\mathbf{p}} d\mathbf{p} G_{n'}(\mathbf{p}, \omega)|^2$ . For the 27th order,

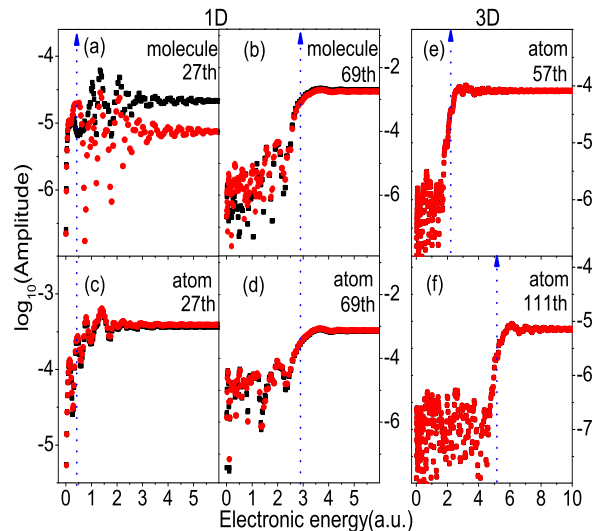


Figure 3: The contribution of  $|\int_0^{\mathbf{p}} d\mathbf{p} G(\mathbf{p}, \omega)|^2$  to certain single harmonic orders for the spectra in Fig. 1(a),(b) and (d). The red curves denote the results obtained with  $n' = 0$ , the black curves denote those obtained with  $n' = 0, 1$ .

in Fig. 3(c) of the atomic case, the red curve shows that the primary contributions of  $|\int_0^{\mathbf{p}} d\mathbf{p} G_0(\mathbf{p}, \omega)|^2$  to this order come from those electrons with a broad energy distribution centered at  $E_{\mathbf{p}}=0.467$  a.u., as indicated by a blue arrow. This energy value agrees with the energy relation  $\omega = 27\omega_0 = E_{\mathbf{p}} + I_p$  ( $\omega_0$  is the laser frequency)[2, 18]. In addition, the black curve of  $n' = 0, 1$  almost superposes the red one. In Fig. 3(a) of the molecular case, the red curve says that the primary contributions come from those electrons with energy smaller than  $E_{\mathbf{p}}=0.467$  a.u.. In Fig. 2(a) there is a dip in the red curve of  $|G_0(\mathbf{p}, \omega)|^2$  around  $E_{\mathbf{p}} = 0.35$  a.u.. We conclude that two-center interference responsible for the dip will induce a strong suppression on this order. Due to the suppression effect, the first excited state will also play an important role in this order. As we can see, the black curve is higher than the red curve here and this order in Fig. 1(a) is strongly suppressed.

For the 69th order, both Fig. 3(b) and (d) show that the primary contributions come from the electrons with a broad energy distribution centered at  $E_{\mathbf{p}} = 2.92$  a.u., as indicated by a blue arrow. This energy value also agrees with the energy relation  $\omega = E_{\mathbf{p}} + I_p$ , but is far from the center of the dip in the red curve in Fig. 2(c). Then we can expect that two-center interference has a trivial influence on this order, and the first excited state plays a negligible role. In Fig. 3(b) of the molecular case, the black curve almost superposes the red curve and this order in Fig. 1(a) is not suppressed.

From Fig. 3(b)-(d), we see that around the blue arrows, there exists a wide energy regime where the in-

tegrated amplitudes increase rapidly. For example, for the 69th order, the regime spreads from  $E_{\mathbf{p}} = 2.5$  a.u. to 3.5 a.u., which converts to the energy of about 17 field-photons. This reveals an important result that continuum electrons with a broad energy distribution contribute equally to one harmonic. The underlying physics is that, from the quantum viewpoint, the recombination electrons probably emit and absorb additional energy from the laser field in the vicinity of the cores[10]. In particular, the blue arrows here indicate the energy  $E_{\mathbf{p}} = \omega - I_p$ . This energy corresponds to the semiclassical energy prediction of  $E[\mathbf{k}(t)] = \omega - I_p$ , obtained in the SFA for the instant momentum  $\mathbf{k}(t)$ [4]. Therefore, our simulations presented here provide a quantitative comparison between the full-quantum energy distribution and the SFA. The comparison gives significant suggestions for proper understandings of the HHG in a full-quantum picture, especially for the intramolecular interference effect, as shown in Fig. 3(a). Our further analyses show that the energy distribution is broader for lower harmonic orders, where the Coulomb potential has a more important role. We expect that the Coulomb effects are mainly responsible for the physics behind our simulations. The differences between the SFA and the TDSE have been reported in some references[19, 20, 21]. In addition, since the center of the broad energy distribution locates at  $E_{\mathbf{p}} = \omega - I_p$ , it confirms the relation  $\omega = E_{\mathbf{p}} + I_p$ , which holds in an averaging process as shown in Ref.[2, 18].

From the above discussions, we anticipate that the two-center interference effect in the molecular HHG not only relies on the population of the first excited state, but also could be affected by laser parameters such as intensity. This is shown in Fig. 1(c). First, the plottings in Fig. 1(c) verify the important role of the first excited state in the molecular HHG. Furthermore, the comparison between the black curves in Fig. 1(a) and (c) reveals that the pronounced minimum in the striking hollow region shifts as the laser intensity changes. Specifically, it shifts from the 27th order in Fig. 1(a) to the 23rd order in Fig. 1(c), as indicated by the vertical arrows. It should be mentioned that in Ref.[5], a spectrum-smoothing procedure is used to help the identification of the interference minima. This procedure is not adopted in our analysis, since we expect a "direct" comparison of the numerical observations and the experimental measurements.

The above interference picture is somewhat different from the point-emitter picture. If we consider that only the electrons, that transit back to the ground state and have the energy  $E_{\mathbf{p}} = \omega - I_p$ , contribute significantly to one harmonic  $\omega$ [5], Eq. 2 can be approximated to  $F(\omega) = \langle 0|\nabla V|\mathbf{p}\rangle \int dt a_0^*(t) e^{i\omega t} c_{\mathbf{p}}(t)$ , with  $\omega = E_{\mathbf{p}} + I_p$ . The above expression explicitly shows that the interference minimum in the molecular HHG spectrum that corresponds to the minimal extremum of the transition dipole  $\langle 0|\nabla V|\mathbf{p}\rangle$  is independent of the laser intensity.

In the full expression of Eq. 2, it says that the electrons, that transit back to varied bound states and

have diverse energy, contribute to one harmonic. Our *ab initio* calculations reveal that the primary contributions to one harmonic come from the recollision electrons with a broad energy distribution, each of which is weighted by the probability amplitude  $G(\mathbf{p}, \omega) = \sum_{n'} \langle n'|\nabla V|\mathbf{p}\rangle \int dt a_{n'}^*(t) e^{i\omega t} c_{\mathbf{p}}(t)$ . This amplitude depends on the laser intensity through the terms  $a_{n'}(t)$  and  $c_{\mathbf{p}}(t)$ . The first excited state also has a nonnegligible role in the molecular HHG. Therefore, the interference minimum in the molecular HHG spectrum could be regulated by the laser intensity. We noted that the cutoff in Fig. 2 of Ref.[8] is probably at the 45th order that corresponds to the laser intensity of  $I = 3 \times 10^{14}$  W/cm<sup>2</sup>. Compared to the intensity of  $I = 2 \times 10^{14}$  W/cm<sup>2</sup> used in Ref.[7], we expect that the uncertain in the calibration of the laser intensity can occur there and the different observations in Ref.[7, 8] can be attributed to the dependence of the interference pattern on the laser intensity.

We now extend our considerations to the 2D and 3D cases. For the 2D  $\text{H}_2^+$ , diagonalizing  $H_0$  becomes computationally intractable, and instead of Eq. 2, we simulate using  $F(\omega) = \int \sum_{n'} a_{n'}^*(t) \langle n'|\vec{\epsilon} \cdot \nabla V|\psi(t)\rangle e^{i\omega t} dt$ . For the 3D hydrogen-like atom, we simulate using  $F(\omega) = \int d\mathbf{p} G(\mathbf{p}, \omega)$  with  $G(\mathbf{p}, \omega) = \sum_{n',l}^{m=0} G_{n',l,m}(\mathbf{p}, \omega)$  and  $G_{n',l,m}(\mathbf{p}, \omega) = \langle n', l, m|\vec{\epsilon} \cdot \nabla V|\mathbf{p}\rangle \int dt a_{n',l,m}^*(t) e^{i\omega t} c_{\mathbf{p}}(t)$ . Here,  $|\mathbf{p}\rangle$  is the accurate continuum state with outgoing wave boundary conditions[21, 22]. The definition of  $n'$  is the same as in the 1D case. These results are presented in Fig. 1(d)-(f). For the 3D atom, Fig. 1(d) shows the applicability of our numerical scheme. Analysis on the integrated contribution of  $|\sum_{n',l}^{m=0} \int_0^{\mathbf{p}} d\mathbf{p} G_{n',l,m}(\mathbf{p}, \omega)|^2$  also obtains the similar results as in the 1D case. We plot the results in the right panels of Fig. 3. For the 2D molecule, Fig. 1(e) and (f) confirm the important role of the excited state in the hollow region (as indicated by the dotted lines) and the shift of the pronounced minimum (from the 39th to the 51st orders as indicated by the solid lines) as the laser intensity changes. These major results are also validated by our further simulations for  $\text{H}_2^+$  with varied internuclear distances. Note that this shift arises from not only the nontrivial role of the excited state in the molecular HHG but also the fact that continuum electrons in a broad energy regime contribute importantly to one harmonic. Even we only consider the transition back to the ground state, the corresponding green curves in the molecular cases in Fig. 1 also reveal the shift of the pronounced minimum. Particularly, all of our 1D and 2D results show that the first excited state already leaves its unambiguous footprints in the molecular HHG spectrum. This finding throws a new light in the difference of the spectral amplitudes for the molecule and its reference atom in the orbital tomography procedure[15].

In summary, we have studied the HHG with a full-quantum treatment. Our simulations revealed a wide regime of continuum electronic energy that contributes significantly to one harmonic, and a nonnegligible contribution of the first excited state to the molecular HHG. Consequently, the two-center interference pattern is in-

fluenced by the laser intensity, as consistent with experiments. These results have important implications for ultrafast imaging of transient molecules.

This work was supported by NNSF(No.10725521),

973 research program No.2006CB921400, 2007CB814800, and grants from the Hong Kong Research Grants Council and Hong Kong Baptist University.

- 
- [\*] Liu\_Jie@iapcm.ac.cn
- [1] M. Hentschel, R. Kienberger, Ch. Spielmann, G. A. Reider, N. Milosevic, T. Brabec, P. Corkum, U. Heinzmann, M. Drescher, and F. Krausz, *Nature* **414**, 509(2001).
- [2] J. Itatani, J. Levesque, D. Zeidler, Hiromichi Niikura, H. Pepin, J. C. Kieffer, P. B. Corkum, and D. M. Villeneuve, *Nature* **432**, 867(2004).
- [3] P. B. Corkum, *Phys. Rev. Lett.* **71**, 1994(1993).
- [4] M. Lewenstein, Ph. Balcou, M. Yu. Ivanov, Anne L’Huillier, and P. B. Corkum, *Phys. Rev. A* **49**, 2117(1994).
- [5] M. Lein, N. Hay, R. Velotta, J. P. Marangos, and P. L. Knight, *Phys. Rev. Lett.* **88**, 183903, (2002); M. Lein, N. Hay, R. Velotta, J. P. Marangos, and P. L. Knight, *Phys. Rev. A* **66**, 023805 (2002); M. Lein, P. P. Corso, J. P. Marangos, and P. L. Knight, *ibid.* **67**, 023819 (2003).
- [6] G. Lagmago Kamta and A. D. Bandrauk, *Phys. Rev. A* **71**, 053407 (2005).
- [7] T. Kanai, S. Minemoto, and H. Sakai, *Nature* **435**, 470(2005).
- [8] C. Vozzi, F. Calegari, E. Benedetti, J.-P. Caumes, G. Sansone, S. Stagira, M. Nisoli, R. Torres, E. Heesel, N. Kajumba, J. P. Marangos, C. Altucci, and R. Velotta, *Phys. Rev. Lett.* **95**, 153902 (2005).
- [9] Anh-Thu Le, X. M. Tong, and C. D. Lin, *Phys. Rev. A* **73** 041402(R) (2006).
- [10] Y. J. Chen and J. Liu, *Phys. Rev. A* **77**, 013410 (2008).
- [11] T. Kanai, S. Minemoto, and H. Sakai, *Phys. Rev. Lett.* **98**, 053002 (2007).
- [12] Xibin Zhou, Robynne Lock, Wen Li, Nick Wagner, Margaret M. Murnane, and Henry C. Kapteyn, *Phys. Rev. Lett.* **100**, 073902 (2008).
- [13] M. F. Ciappina, C. C. Chirilă and M. Lein, *Phys. Rev. A* **75**, 043405 (2007).
- [14] S. Baker, J. S. Robinson, M. Lein, C. C. Chirilă, R. Torres, H. C. Bandulet, D. Comtois, J. C. Kieffer, D. M. Villeneuve, J. W. G. Tisch, and J. P. Marangos, *Phys. Rev. Lett.* **101**, 053901 (2008).
- [15] Y. Chen, Y. Li, S. Yang, and J. Liu, *Phys. Rev. A* **77**, 031402(R) (2008).
- [16] D. B. Milošević, G G Paulus, D Bauer and W Becker, *J. Phys. B* **39** R203-R262 (2006).
- [17] J. Muth-Böhm, A. Becker, and F. H. M. Faisal, *Phys. Rev. Lett.* **85**, 2280(4) (2000).
- [18] J. Levesque, D. Zeidler, J. P. Marangos, P. B. Corkum, and D. M. Villeneuve, *Phys. Rev. Lett.* **98**, 183903 (2007).
- [19] Zhangjin Chen, Toru Morishita, Anh-Thu Le, M. Wickenhauer, X. M. Tong, and C. D. Lin, *Phys. Rev. A* **74** 053405 (2006).
- [20] J. Tate, T. Augustine, H. G. Muller, P. Salières, P. Agostini, and L. F. DiMauro, *Phys. Rev. Lett.* **98**, 013901 (2007); K. Schiessl, K. L. Ishikawa, E. Persson, and J. Burgdörfer, *ibid.* **99**, 253903(2007); M. V. Frolov, N. L. Manakov, and Anthony F. Starace, *ibid.* **100**, 173001 (2008).
- [21] X. M. Tong, S. Watahiki, K. Hino, and N. Toshima, *Phys. Rev. Lett.* **99**, 093001 (2007).
- [22] Toru Morishita, Anh-Thu Le, Zhangjin Chen, and C. D. Lin, *Phys. Rev. Lett.* **100**, 013903 (2008).